Engineering Failure Analysis 126 (2021) 105465

Contents lists available at ScienceDirect

Engineering Failure Analysis

journal homepage: www.elsevier.com/locate/engfailanal

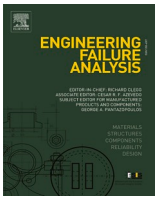

Irreversible interfacial slip in shrink-fitted bimetallic work roll promoted by roll deformation

Nao-Aki Noda *, Rahimah Abdul Rafar *, Hiromasa Sakai, Xuchen Zheng, Hiroyuki Tsurumaru, Yoshikazu Sano, Yasushi Takase

Mechanical Engineering Department, Kyushu Institute of Technology, 1-1 Sensui-cho, Tobata, Kitakyushu, Fukuoka 804-8550, Japan

ARTICLE INFO

Keywords:
Bimetallic roll
Shrink-fitted
Irreversible relative displacement
Interfacial slip
FEM analysis

ABSTRACT

Shrink-fitted sleeve rolls have several advantages; for example, the shaft can be reused after reaching the threshold minimum diameter. However, the interfacial slip sometimes appears between the shaft and the shrink-fitted sleeve causing roll damage. To clarify the interfacial slip in real rolls, in this study, FEM analysis is performed focusing on the roll deformation promoting the failure. The irreversible relative displacement between the shaft and the sleeve may cause the interfacial slip when the roll is deformed under external loading. The amount of the interface slip increases significantly with increasing the shaft deformation by decreasing Young's modulus of the shaft.

1. Introduction

In metalworking, rolling processes are more tonnage than any other manufacturing process. Rolling technology is developing and advancing further although seemingly mature [1–15]. Fig. 1 illustrates the rolling roll in roughing stands of hot rolling stand mills. The rolls are classified into two types; one is a single-solid type, and the other is a shrink-fitted assembled type consisting of a sleeve and a shaft.

Some sleeve rolls are practically and successfully used as the back-up rolls having large trunk diameter exceeding 1000 mm and also used as the rolling rolls for large H-section steel [1–3]. Those sleeve rolls have several advantages. The shaft can be reused by replacing the sleeve after consumed due to the abrasion or the surface roughening. Furthermore, the sleeve wear resistance can be improved independently without loosening the shaft ductility.

On the other hand, this shrink-fitted sleeve roll has several peculiar problems such as residual bend deformation, fretting fatigue cracks at the sleeve end and sleeve fracture due to the circumferential sleeve slippage [5–13]. Among them, no detail studies are available for this circumferential slippage in rolling roll. It should be noted that the circumferential slippage sometimes occurs even though the resistance torque at the interface is larger than the motor torque. It is known that this slippage is irreversible since the slippage does not go back to the initial state in a reversible way after removing the load. Since the initial conditions cannot be restored exactly [12–15] this phenomenon is hard to be proved. Considering no quantitative study available for rolling rolls, our previous study assumed a rigid shaft to simplify the phenomenon and to realize the slippage in the numerical simulation [12–15]. However, similar phenomenon is known as "interfacial creep" in ball bearing. In this failure, the bearing gradually moves circumferentially to the stationary shaft or housing [16–26]. To explain this failure, Soda [16] explained two factors; one is the clearance between the ring and

* Corresponding authors.
E-mail addresses: noda.naoaki844@mail.kyutech.jp (N.-A. Noda), rafar.rahimah-binti485@mail.kyutech.jp (R. Abdul Rafar).

https://doi.org/10.1016/j.engfailanal.2021.105465
Received 22 October 2020; Received in revised form 20 April 2021; Accepted 6 May 2021
Available online 11 May 2021
1350-6307/

the shaft or housing, and the other is the elastic deformation which Imai [17] proved experimentally. Those studies treated the interface creep in the opposite direction to the bearing rotation [17,18] but another reports treated the creep in the same direction [19,20]. Several other studies are also available for the bearing creep phenomenon [21–28]. However, few studies discussed the phenomenon quantitatively.

In this study, to understand the phenomena essentially, the elastic roll deformation effect will be discussed in the simulation under free rolling. Furthermore, by using miniature rolling facility, the interfacial slip will be verified experimentally. Different from ball bearings, as shown in Fig. 1a, the driving torque and the frictional force may promote the slippage in the sleeve rolls causing serious failure. However, before considering additional factors such as the motor torque, it is necessary to investigate and verify the essence of the phenomena under free rolling like ball bearing creep. By clarifying the phenomenon, in this way, such unknown failure can be prevented in the near future and the sleeve assembly type roll can be used much more widely.

2. Interfacial slip simulation focusing on the relative displacement

Fig. 1 illustrates a sleeve assembly type roll used in rolling. Fig. 1a illustrates the central cross section and Fig. 1b illustrates the axial cross section. As shown in Fig. 1, the sleeve roll consists of a sleeve and a shaft shrink-fitted. Fig. 1c shows an example of a commonly used bimetallic sleeve roll manufactured by centrifugal casting method. Here, the outer layer is made of high-speed steel (HSS) having high abrasion resistance and the inner layer is made of ductile casting iron (DCI) having high ductility. In this study a single material sleeve roll is considered instead of the bimetallic roll to simplify the analysis and to clarify the interfacial slip.

As shown in Fig. 1a, the roll is subjected to the contact force P from the back-up roll, the rolling force P_h and the frictional force S from the rolling plate. Since two-dimensional modelling is applied, the external force per unit length should be considered as well as motor torque T. In Fig. 1b, the back-up roll is longer than the width the rolling plate; and therefore, the bending force P_b is acting at the bearing. Here, the rolling force P, the rolling reaction force P_h and the bending force P_b should be balanced, but P_b is estimated to be <10% of P and P_h [5]. Therefore, in this study, assume the bending force $P_b = 0$; then, the rolling force ($=\sim P \times$ back-up roll body length) is equal to the rolling force ($=\sim P_h \times$ strip width) as $P \simeq P_h$. This modelling refers to the case study of the loading at the fifth stage of hot finishing roll [5].

Fig. 2 illustrates two-dimensional modelling in numerical simulation. As shown in the Appendix A in detail, the roll rotation is expressed by the load shifting on the fixed roll surface [12–15]. Fig. 2a illustrates the real roll by shifting the load on the roll surface with the roll center fixed. The roll is assumed to be subjected to the concentrated rolling load $P = 13270$ N/mm [4,5]. In rolling the friction S is used to compress the rolling plate between the rolls. In this study, however, the free rolling with $T = 0$ and $S = 0$ will be discussed as shown in Fig. 2b. This is similar to the ball bearing where the torque is not applied on the ball but either on the inner or

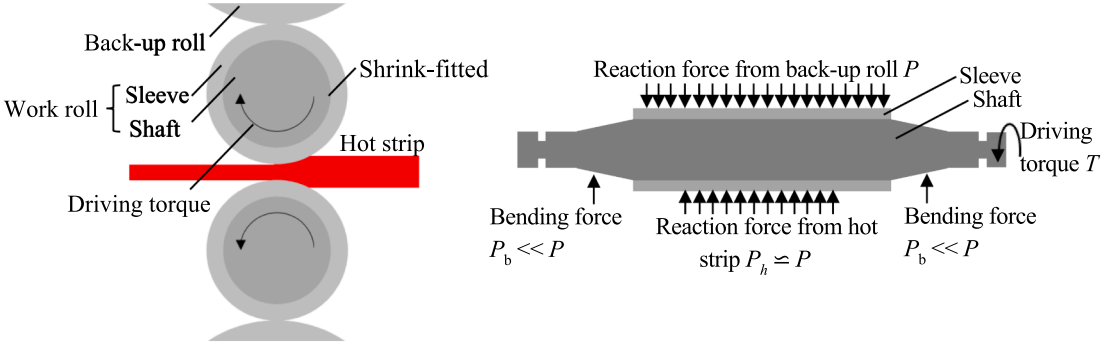

(a) Central cross section view of rolling roll. (b) Axial section view of rolling roll.

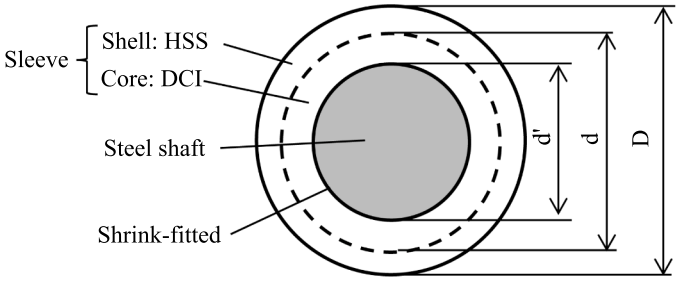

(c) A target of this study: HSS bimetallic roll in central cross section.

Fig. 1. Schematic illustration for real hot strip rolling roll.

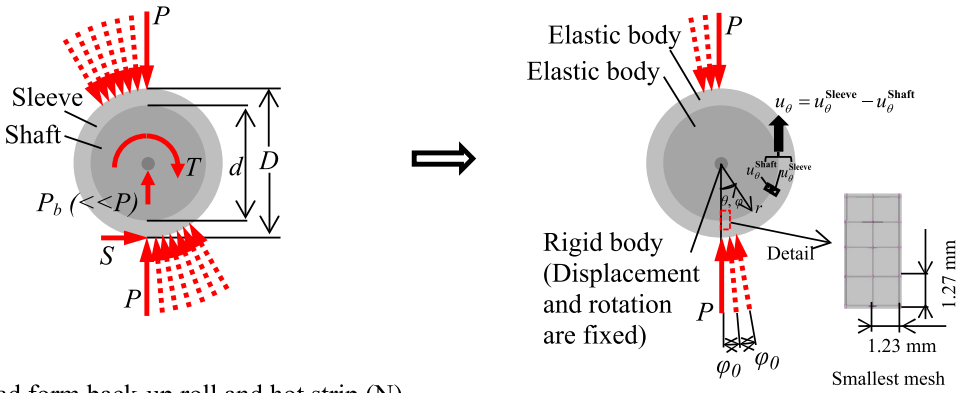

P: Load form back-up roll and hot strip (N)
S: Frictional force (N)
P_b: Bending force from bearing (N) <<*P*
T: Driving torque (Nm) = *SD*/2

(a) Real roll.

θ: Circumferential angle of sleeve
φ_0: Load shift interval
φ: Load shift angle

(b) Roll model (*T*, *S*, $P_b = 0$).

Fig. 2. Modelling and simulation for interfacial slip.

outer ring and the balls freely rotates to minimize the friction. Fig. 2b also shows an example of the mesh division for the finite element method (FEM). To realize the interface slippage, the FEM simulation should be well conducted on basis of the experience and skills for engineering applications. In the previous studies [29–32], the FEM mesh error was discussed for bonded problems and mesh-independent technique was proposed confirming that the displacement boundary condition applied confirming that the displacement boundary condition is relatively insensitive. Contact status change was clarified when the pitch-difference nut is tightened [33] and dynamic deformation was investigated through consecutive quasi-static analyses [34]. On the basis of those skills, during the ceramic roll rotation, the axial movement of the shaft was analyzed by shifting the load on the fixed shaft [35–38]. In this study, the circumferential sleeve slippage will be realized by extending the above technique and applying FEM code Marc/Mentat 2012 to the elastic contact quasi-static analysis for rolling rolls. In this code, the complete Newton-Raphson method and the direct constraint method for the contact analysis are used. As shown in Fig. 2b, a 4-node quadrilateral plane strain is used with the number of mesh elements are 309,440 with confirming the mesh independency of the results [39].

Table 1 shows mechanical properties, dimensions and boundary conditions of the model in Fig. 2b. The loading condition used in this study is based on the data at No. 5 stand for roll hot strip finishing roll mill [4,5]. Assume the concentrated loading *P* from the back-up roll and the reaction *P* from the strip with $P = 13270$ N/mm [4,5]. Small effect can be confirmed by replacing Hertzian contact stress with the concentrated force *P*. The shrink-fitting ratio is defined as δ/d, where δ is the diameter difference between the inner diameter of the sleeve and the outer diameter of the shaft. Usually, the shrink-fitting ratio in the range $\delta/d = 0.4 \times 10^{-3} \sim 1.0 \times 10^{-3}$ is applied to sleeve rolls on the basis of long year experience. This is because a smaller value $\delta/d < 0.4 \times 10^{-3}$ may cause interface slip easily and a larger value δ/d greater than 1.0×10^{-3} may increase the risk of sleeve fracture [6]. To study the irreversible interfacial slip, in this paper, $\delta/d = 0.5 \times 10^{-3}$ is focused. The effect of the shrink-fitting ratio is discussed in Appendix B. Regarding the friction coefficient μ controlling the slippage resistance on the interface, $\mu = 0.2$ was used in an experimental study and $\mu = 0.4$ was often used for steel surfaces previously [1,40]. In this way, since $\mu = 0.2 \sim 0.4$ is usually used for sleeve assembly type rolls, in this study, the friction coefficient $\mu = 0.3$ between the sleeve and the shaft is used.

Table 1
Mechanical properties, dimensions and boundary conditions in Fig. 2b [13–15].

Mechanical properties	Sleeve	Young's modulus of steel sleeve E_{sleeve}	210 GPa
		Poisson's ratio of steel sleeve ν	0.28
	Shaft	Young's modulus of elastic shaft E_{shaft}	210 GPa
		Poisson's ratio of steel shaft ν	0.28
Roll size		Outer diameter of sleeve	700 mm
		Inner diameter sleeve *d*	560 mm
Shrink fitting		Shrink fitting ratio δ/d	0.5×10^{-3}
		Friction coefficient between sleeve and shaft μ	0.3
External force		Concentrated load per unit thickness *P*	13270 N/mmTotal: 1.327×10^7 NRolled width: 1000 mm
		Frictional force per unit thickness *S*	0 N/mm
		Motor torque per unit thickness *T*	0 N/mm
		Bending force from bearing P_b	0 N/mm

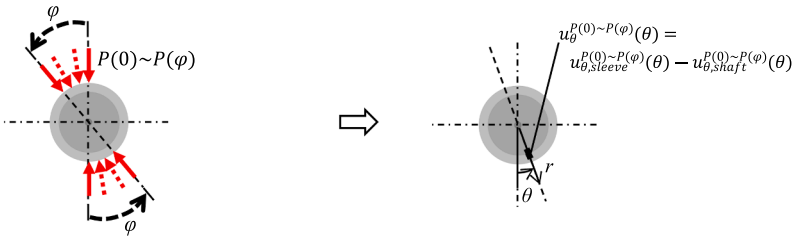

(i) Define the pair of the loads shift from $\varphi = 0$ to φ, and $\varphi = \pi$ to $(\pi + \varphi)$ as $P(0)\sim P(\varphi)$.

(ii) Define the displacement $u_\theta(\theta)$ due to $P(0)\sim P(\varphi)$ as $u_\theta^{P(0)\sim P(\varphi)}(\theta)$.

(a) Definition of interfacial displacement $u_\theta^{P(0)\sim P(\varphi)}(\theta)$ due to the load shifting $P(0)\sim P(\varphi)$.

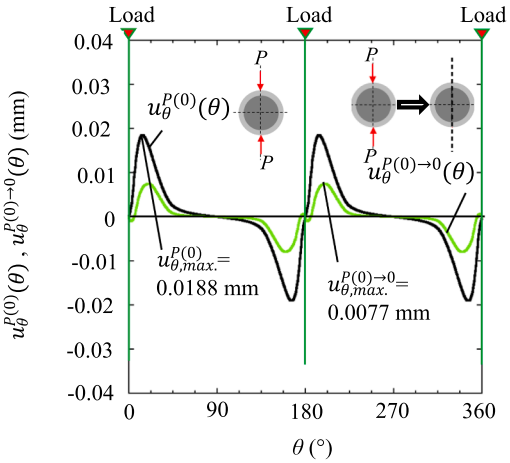

b) Interfacial displacement $u_\theta^{P(0)}(\theta)$ due to the initial load $P(0)=P$ and irreversible interfacial displacement $u_\theta^{P(0)\to 0}(\theta)$ after removing the initial load $P(0)$ as $P(0)\to 0$ when $E_{shaft} = E_{sleeve} = 210$ GPa.

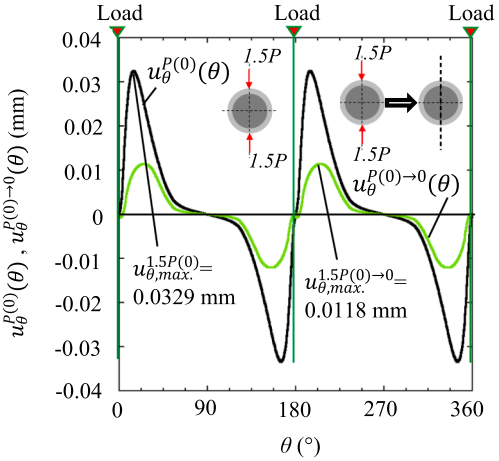

c) Interfacial displacement $u_\theta^{P(0)}(\theta)$ due to the initial load $P(0)=1.5P$ and irreversible interfacial displacement $u_\theta^{P(0)\to 0}(\theta)$ after removing the initial load $P(0) = 1.5P$ as $P(0)\to 0$ when $E_{shaft} = E_{sleeve} = 210$ GPa.

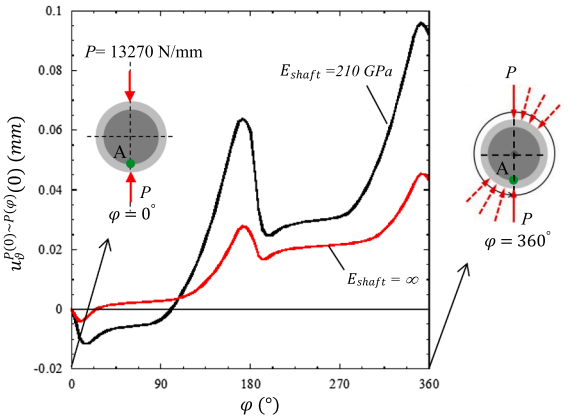

(d) Interfacial displacement $u_\theta^{P(0)\sim P(\varphi)}(0)$ due to the load shifting $P(0)= P$ from from $\varphi = 0$ to $\varphi = \varphi$ when $E_{shaft} = E_{sleeve} = 210$ GPa and when $E_{shaft} = \infty$ and $E_{sleeve} = 210$ GPa.

Fig. 3. Interfacial displacement and irreversible interfacial displacement.

3. Irreversible relative displacement causing interfacial slip

The relative displacement accumulation between the sleeve and shaft may represent the interfacial slip. In Fig. 3a, the relative displacement $u_\theta^{P(0)\sim P(\varphi)}(\theta)$ due to the load shifting $P(0) \sim P(\varphi)$ is defined between the sleeve and shaft when the load moves from the angle $\varphi = 0$ to $\varphi = \varphi$. Here, notation φ denotes the angle where the load is shifting and notation θ denotes the position where the displacement is evaluated. The load $P(\varphi)$ is defined as the pair of forces acting at $\varphi = \varphi$ and $\varphi = \varphi + \pi$. The notation $u_\theta^{P(0)\sim P(\varphi)}(\theta)$ means the relative displacement $u_\theta(\theta)$ at $\theta = \theta$ when the pair of loads are applied at $\varphi = 0$ to $\varphi = \varphi$ and $\varphi = \pi$ to $\varphi = \varphi + \pi$.

Fig. 3b illustrates an example of the interfacial displacement $u_\theta^{P(0)}(\theta)$ due to an initial load $P(0)$ when E_{shaft}=E_{sleeve} = 210 GPa. Fig. 3b also indicates the displacement $u_\theta^{P(0)\to 0}(\theta)$, which is the residual displacement when the initial load $P(0)$ is removed as $P(0) \to 0$. As shown in Fig. 3, $u_\theta^{P(0)\to 0}(\theta)$are not zero as well as $u_\theta^{P(0)}(\theta)$. This non-zero $u_\theta^{P(0)\to 0}(\theta)$means the displacement $u_\theta^{P(0)}(\theta)$ and $u_\theta^{P(0)\sim P(\varphi)}(\theta)$ is irreversible. Fig. 3c shows $u_\theta^{P(0)}(\theta)$and $u_\theta^{P(0)\to 0}(\theta)$when the larger load $P(0) = 1.5P$ is applied and removed as $P(0) \to 0$. The maximum value of the slip $u_\theta^{P(0)}(\theta)$ increases from 0.0329/0.0188≈1.75, which is larger than 1.5. This non-linearity is caused by contact status change although the displacement is elastic. The maximum value of the irreversible slip $u_\theta^{P(0)\to 0}(\theta)$ increases from 0.0118/0.0077≈1.53, which is also larger than 1.5. Fig. 3b and c illustrates the irreversible displacement $u_\theta^{P(0)\to 0}(\theta)$in a fundamental way by removing the initial load completely. During the roll rotation that can be expressed as the load shifting, such irreversible displacement is accumulated and appears in a complicated way.

When the load is shifted from$\varphi = 0$ to $\varphi = 2\pi$, Fig. 3d illustrates the relative displacement $u_\theta^{P(0)\sim P(\varphi)}(0)$ at $\theta = 0$. As shown in Fig. 3b, under the initial load$u_\theta^{P(0)}(0) = 0$. Due to the irreversible slip, $u_\theta^{P(0)\sim P(\varphi)}(0)$ becomes negative as$u_\theta^{P(0)\sim P(\varphi)}(0) < 0$ in the range $0< \varphi \leq 96^\circ$ and becomes positive $u_\theta^{P(0)\sim P(\varphi)}(0) \geq 0$ in the range $\varphi > 96^\circ$ when $E_{shaft} = E_{sleeve}$= 210 GPa. Since the slip varies depending on θ, the variations are indicated in Appendix A for half rotation as $u_\theta^{P(0)\sim P(\pi)}(\theta)$ and for one rotation as $u_\theta^{P(0)\sim P(2\pi)}(\theta)$ in the range $\theta = 0 \sim 2\pi$. To express the amount of the slip with increasing φ, the average displacement can be defined by the following equation.

$$u_{\theta,ave.}^{P(0)\sim P(\varphi)} = \frac{1}{2\pi}\int_0^{2\pi} u_\theta^{P(0)\sim P(\varphi)}(\theta)d\theta \tag{1}$$

As shown in Fig. 3, when the initial load P is applied at $\varphi = 0$, the average displacement is zero as $u_{\theta,ave.}^{P(0)} = 0$. Also, when the initial load is removed as $P(0) \to 0$ the average displacement is zero as $u_{\theta,ave.}^{P(0)\to 0} = 0$.It should be noted that the displacements themselves $u_\theta^{P(0)}(\theta)$ and $u_\theta^{P(0)\to 0}(\theta)$are not zero except at $\theta = 0$, π, and 2π. This non-zero displacement means once the load is applied, such local slippage may appear. Although $u_\theta^{P(0)}(\theta)$ is symmetric as shown in Fig. 3b, with increasing the load shifting angle φ, the average displacement $u_{\theta,ave.}^{P(0)\sim P(\varphi)}$ increases after losing the symmetry (see Fig. A.2 in Appendix A).

Fig. 4 illustrates the average displacement $u_{\theta,ave.}^{P(0)\sim P(\varphi)}$ by varying Young's modulus of the shaft, E_{shaft}. As indicated in Fig. 4 and Table 2, assumed shaft materials are ductile cast iron (DCI), steel, cermet and rigid. Table 2 also indicates the shrink-fitting stress $\sigma_{r_{shrink}}$

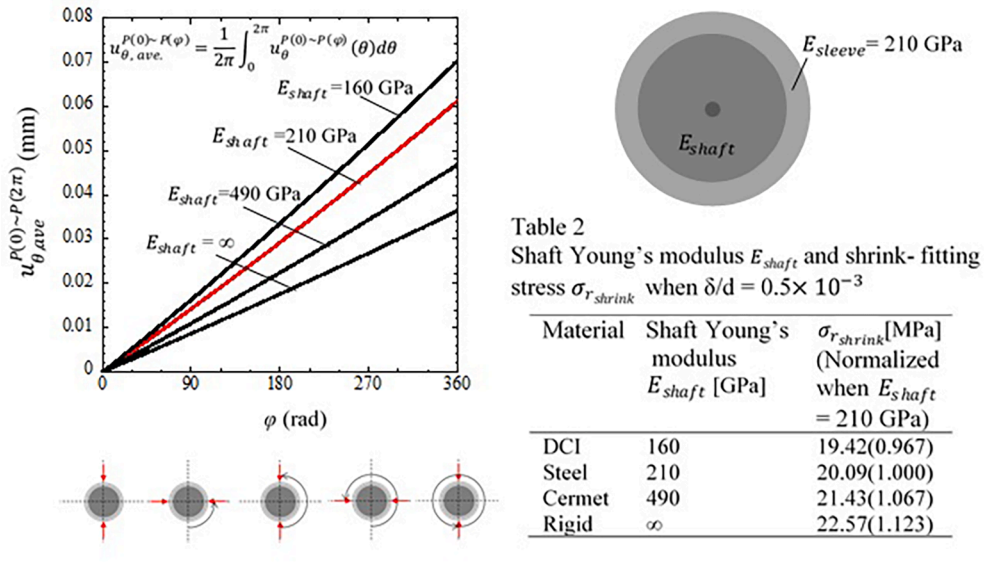

Table 2
Shaft Young's modulus E_{shaft} and shrink- fitting stress $\sigma_{r_{shrink}}$ when δ/d = 0.5× 10^{-3}

Material	Shaft Young's modulus E_{shaft} [GPa]	$\sigma_{r_{shrink}}$[MPa] (Normalized when E_{shaft} = 210 GPa)
DCI	160	19.42(0.967)
Steel	210	20.09(1.000)
Cermet	490	21.43(1.067)
Rigid	∞	22.57(1.123)

Fig. 4. Average displacement $u_{\theta,ave.}^{P(0)\sim P(2\pi)}(\theta)$ increases almost linearly with increasing load shift angle ϕ.

Table 2
Shaft Young's modulus $E_{shaft}$and shrink- fitting stress $\sigma_{r_{shrink}}$ when $\delta/d = 0.5 \times 10^{-3}$

Material	Shaft Young's modulus E_{shaft} [GPa]	$\sigma_{r_{shrink}}$ [MPa] (Normalized when E_{shaft} = 210 GPa)
DCI	160	19.42(0.967)
Steel	210	20.09(1.000)
Cermet	490	21.43(1.067)
Rigid	∞	22.57(1.123)

by varying E_{shaft}. The average displacement $u_{\theta,ave.}^{P(0)\sim P(\varphi)}$increases with increasing the load shift angle φ. With decreasing E_{shaft}, the shrink-fitting stress $\sigma_{r_{shrink}}$ decreases slightly as shown in Table 2. It should be noted that the average displacement $u_{\theta,ave.}^{P(0)\sim P(\varphi)}$ is accelerated more significantly with decreasing E_{shaft}. The interface slip may occur as soon as the load shifting starts. It should be noted that the amount of interfacial slip $u_{\theta,ave.}^{P(0)\sim P(\varphi)}$ increases almost linearly with increasing the load shift angle φ as shown in Fig. 4. In the following, therefore, the load shift $P(0) \sim P(2\pi)$ which represents one rotation load will be considered to discuss the interfacial slip since the results under many rotations can be linearly estimated.

Fig. 5 illustrates the average displacement $u_{\theta,ave.}^{P(0)\sim P(2\pi)}$ due to the load shifting $P(0) \sim P(2\pi)$ versus the shaft Young's modulus E_{shaft}. The average displacement for ductile iron (DCI) is larger compared to steel, cermet and rigid shaft. It may be concluded that the shaft elastic deformation contributes to the interfacial slip. In the following section, the effect of the shaft materials to the interfacial slip will be discussed in detail. The relation between $u_{\theta,ave.}^{P(0)\sim P(2\pi)}$ and E_{shaft} in Fig. 5 should be compared with other relations to find out the controlling parameter of $u_{\theta,ave.}^{P(0)\sim P(2\pi)}$ (see Fig. 7, Fig. 8, Fig. 10).

4. Discussion of shaft elastic deformation on interfacial slip

Fig. 6 shows the shear stress distribution $\tau_{r\theta}^{P(0)\sim P(2\pi)}$ in comparison with the frictional stress $\mu\sigma_r^{P(0)\sim P(2\pi)}$ along the shrink-fitting surface. Fig. 6a shows the rigid shaft result under the load shifting $P(0) \sim P(2\pi)$. Fig. 6b shows the elastic shaft result whenE_{shaft} = 210 GPa under the load shifting $P(0) \sim P(2\pi)$. The notation $P(0) \sim (2\pi)$ denotes one rotation loading from $\varphi = 0$ to $\varphi = 2\pi$. It should be noted that the displacement increases with increasing φ as shown in Fig. 4 but the stresses σ_θ does not change with increasing φ [13].

In this study, the friction coefficient $\mu = 0.3$ is assumed between the sleeve and the shaft. By considering the FEM accuracy, the irreversible relative displacement may appear when $\tau_{r\theta} \cong |\mu\sigma_r|$ within the error ± 1 MPa. This region can be defined as the slippage region ℓ_{slip}. In the previous study by Noda et. al. [12], the region was named "quasi-equilibrium stress zone $\tau_{r\theta} \cong |\mu\sigma_r|$" where the irreversible displacement occurs. As shown in Fig. 6a and b, the slippage region ℓ_{slip} is much larger for the elastic shaft compared to the rigid shaft. This behaviour explained the larger irreversible displacement appears as shown in Fig. 5.

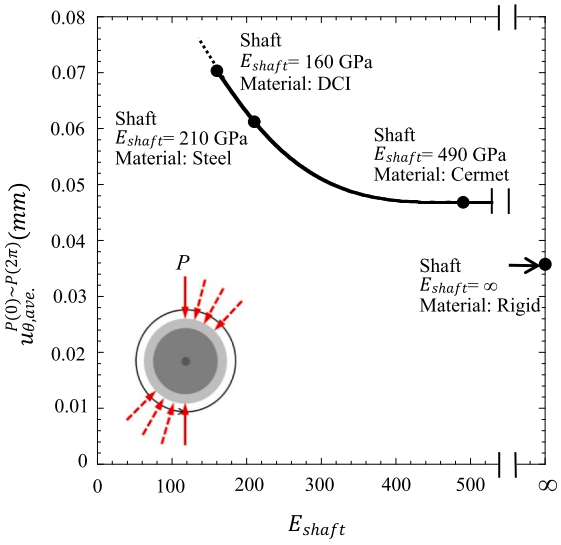

Fig. 5. Average displacement $u_{\theta,ave.}^{P(0)\sim P(2\pi)}$ versus E_{shaft} whenE_{sleeve} = 210 GPa.

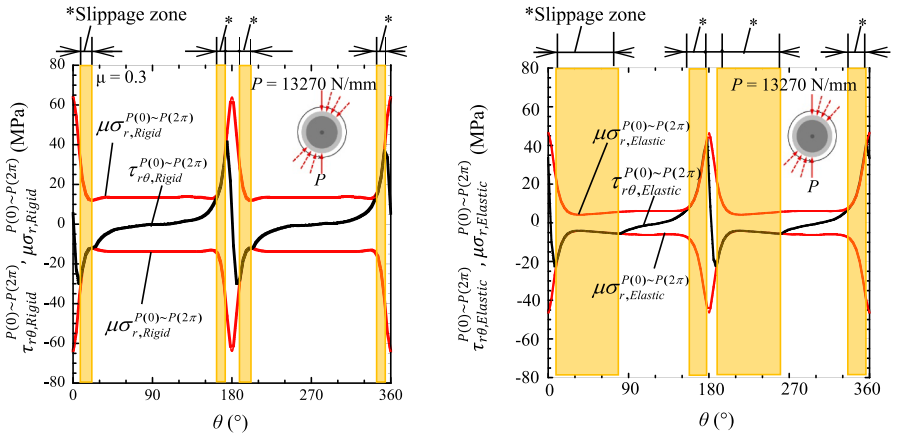

(a) Rigid shaft under the load shifting $P(0)\sim P(2\pi)$.

(b) Elastic shaft when E_{shaft}= 210 GPa under the load shifting $P(0)\sim P(2\pi)$.

Fig. 6. Comparison of slippage zone of rigid shaft and elastic shaft under the load shifting $P(0) \sim P(2\pi)$.

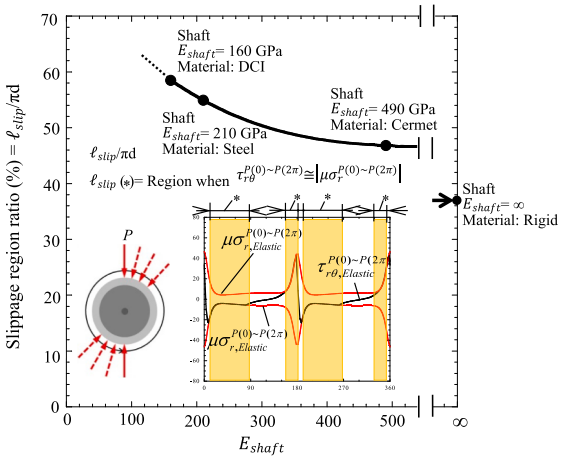

Fig. 7. Slippage range ratio $\ell_{slip}/\pi d$ versus E_{shaft} whenE_{sleeve} = 210 GPa.

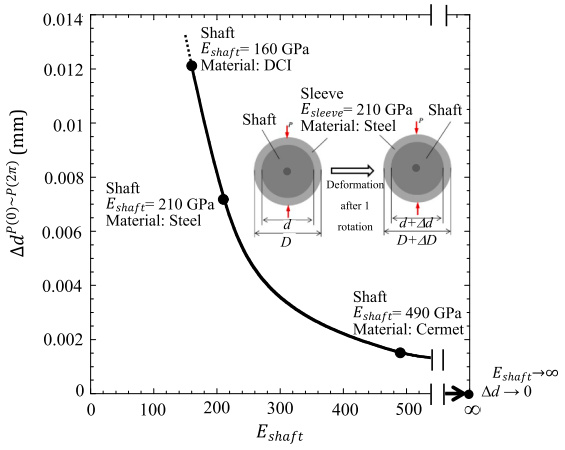

Fig. 8. Shaft diameter increment $\Delta d^{P(0)\sim P(2\pi)}$ versus E_{shaft} whenE_{sleeve} = 210 GPa.

Fig. 7 shows the slippage region ratio that is defined as $\ell_{slip}/\pi d$ due to the load shifting $P(0) \sim P(2\pi)$. Here the slippage region ℓ_{slip} is where $\tau_{r\theta}^{P(0)\sim P(2\pi)} \cong \left|\mu\sigma_r^{P(0)\sim P(2\pi)}\right|$.

$$\text{Slippage region ratio} = \ell_{slip}/\pi d$$

$$\ell_{slip} = \text{Region where } \tau_{r\theta}^{P(0)\sim P(2\pi)} \cong \mu\sigma_r^{P(0)\sim P(2\pi)} \tag{2}$$

As shown in Fig. 7, the slippage region ratio $\ell_{slip}/\pi d$ decreases with increasing E_{shaft}. As shown in Fig. 5, the average displacement $u_{\theta,ave.}^{P(0)\sim P(2\pi)}$ also decreases with increasing E_{shaft}. In this way, the interfacial displacement may be promoted by larger elastic deformation due to smaller E_{shaft}. Therefore, the reason why $\ell_{slip}/\pi d$ decreases with increasing E_{shaft} is discussed in this section.

First, as a typical elastic deformation, the diameter increase in the lateral direction Δd is focused. Fig. 8 shows the lateral diameter increment $\Delta d^{P(0)\sim P(2\pi)}$ after the one cycle loading $P(0) \sim P(2\pi)$ when the final loads are applied in the vertical direction at $\theta = 0°$ and $\theta = 180°$. With increasing E_{shaft}, the lateral diameter increment $\Delta d^{P(0)\sim P(2\pi)}$ decreases and goes to zero. Figs. 7 and 8 show the same trend although in Fig. 8 $\Delta d \to 0$ when $E_{shaft} \to \infty$. It can be concluded that the interfacial slip can be accelerated by the larger elastic shaft deformation due to smaller E_{shaft}.

Next, the contact stress change due to the external loading is focused. Fig. 9 illustrates the contact stress $\sigma_r^{P(0)\sim P(2\pi)}$ along the interface due to the load shifting $P(0) \sim P(2\pi)$. As shown in Fig. 9, there is the region ℓ_{small} where the contact stress $\sigma_r^{P(0)\sim P(2\pi)}$ becomes smaller than the original shrink-fitted stress $\sigma_{r_{shrink}}$ as $\sigma_r^{P(0)\sim P(2\pi)} \leqq \sigma_{r_{shrink}}$. Here, $\sigma_{r_{shrink}}$ denotes the shrink-fitting stress without applying the load P when $E_{shaft} = E_{sleeve} = 210$GPa. The region ℓ_{small} can be named "the smaller contact stress region" where $\sigma_r^{P(0)\sim P(2\pi)} \leqq \sigma_{r_{shrink}}$. In Fig. 9, the length of the smaller contact stress region ℓ_{small} is express as $\ell_{small} = \theta_{small} \times d/2$ by using the angle θ_{small} as described in Fig. 10. As shown in Fig. 9, the DCI shaft has a larger ℓ_{small} followed by steel and cermet shaft, while rigid shaft has a smallest ℓ_{small}.

Fig. 10 shows the smaller contact stress region ratio $\ell_{small}/\pi d$ normalized by the total circumferential length πd by varying E_{shaft}. The smaller contact stress region ratio is given by the following equation.

$$\text{Smaller contact stress region ratio} = \ell_{small}/\pi d$$

$$\ell_{small} = \text{Region where } \sigma_r^{P(0)\sim P(2\pi)} \leqq \sigma_{r_{shrink}} \text{ when } E_{shaft} = E_{sleeve} = 210\ GPa \tag{3}$$

The ratio $\ell_{small}/\pi d$ increases with decreasing E_{shaft}. Similar trend can be seen for $\ell_{slip}/\pi d$ in Fig. 7. With increasing the smaller contact stress region, the slippage may happen easily. It can be concluded that the slippage region ℓ_{slip} is closely related to the smaller contact stress region ℓ_{small}.

In this paper, under fixed $E_{sleeve} = 210$ GPa, the interfacial slip is discussed by varying E_{shaft} as shown in Table 2. One may think that E_{shaft} assumed in Figs. 4–10 is not very realistic; and instead, larger E_{sleeve} such as ceramics sleeve should be discussed to reduce the surface wear. In this paper, however, to develop the bimetallic sleeve roll in Fig. 1c, the effect of the shaft elastic deformation on the interface slippage is focused to clarify the phenomena. After understanding the essential phenomena in this way, the interface slippage will be prevented.

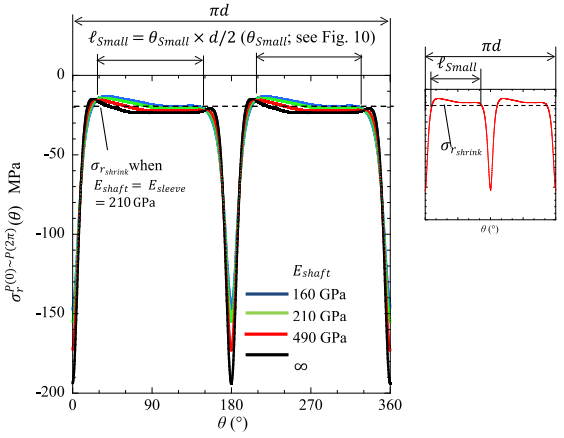

Fig. 9. Definition of smaller contact stress region ℓ_{small} where $\sigma_r^{P(0)\sim P(2\pi)} \leqq \sigma_{r_{shrink}}$.

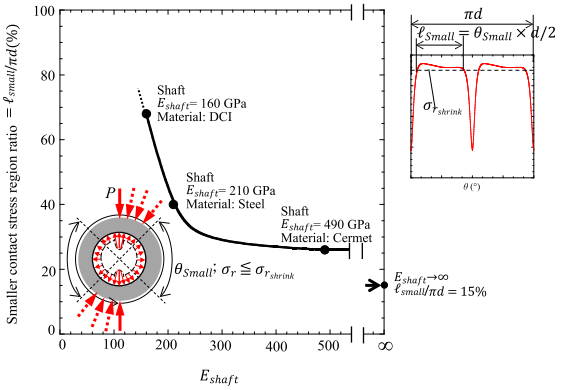

Fig. 10. Smaller contact stress region ratio $\ell_{small}/\pi d$versus E_{shaft} whenE_{sleeve} = 210 GPa.

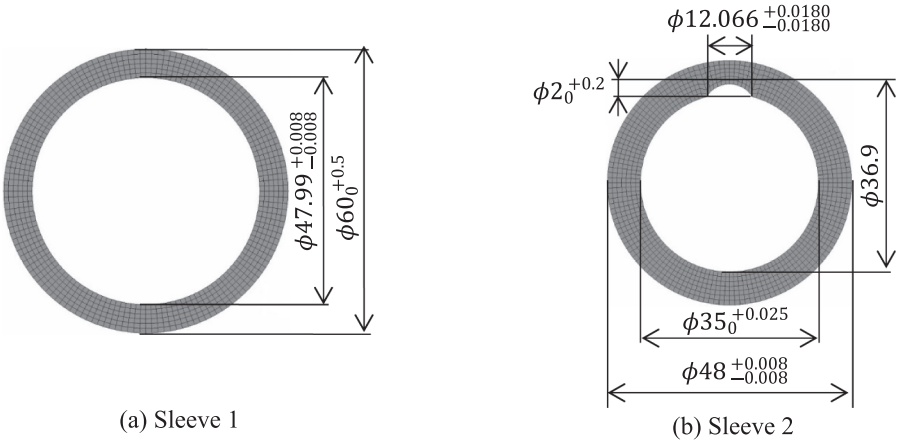

Fig. 11. FEM mesh.

5. Experimental confirmation

The relative displacement was discussed as described in the above sections. In this section, the interfacial slip will be confirmed experimentally. Fig. 11 shows the FEM mesh of a miniature roll used in this experiment. A 4-node quadrilateral plane strain element is used for mesh division, and the number of mesh elements are 7408. By using the miniature roll whose diameter is 60 mm, the experiment is conducted under free rolling with $T = 0$ and $S = 0$. The work roll consists of two sleeves and a shaft. To realize the slip between sleeve 1 and sleeve 2 as shown in Fig. 11, sleeve 2 and shaft are fixed by the key. Assume the loading $P = 490$ N/mm, the shrink-fitting ratio $\delta/d = 0.2 \times 10^{-3}$ and the friction coefficient $\mu = 0.3$ between sleeve 1 and sleeve 2, the numerical simulation is newly performed for the miniature roll. Similar to Fig. 3b, $u_{\theta}^{P(0)\sim P(\varphi)}(\theta)$ is defined as the relative displacement between sleeve 1 and sleeve 2.

Table 3 shows a summary of the average displacement values obtained through the results of the experiment and simulation when the shrink-fitting ratio $\delta/d = 0.2 \times 10^{-3}$ for the miniature roll. The experimental value corresponding to $u_{\theta,ave.}^{P(0)\sim P(2\pi)}$, which is the average displacement during one roll rotation that can be calculated in the following way.

Table 3
Comparison of experimental data and simulation results for average displacement.

	Shrink-fitting ratio $\delta/d = 0.2 \times 10^{-3}$	
	Experiment data	Simulation results
$u_{\theta,ave.}^{P(0)\sim P(2\pi)}$	0.108×10^{-2} mm	0.886×10^{-2} mm

$$u_{\theta,ave.}^{P(0)\sim P(2\pi)} = \frac{\theta_{slip} \times \pi \mathrm{d}}{360^\circ \times \pi} = \frac{77^\circ \times \pi \times 48mm}{360^\circ \times 3 \times 10^4} = \frac{32mm}{3 \times 10^4} = 0.108 \times 10^{-2} mm \tag{4}$$

In Eq. (4), θ_{slip} is the slip angle observed in the experiment, d is the inner diameter of sleeve 1 and n is the number of the roll rotation. As shown in Table 3, the order of the numerical simulation coincides with the order of the experimental result. The experimental observation shows several small local scratches and developed damage can be seen on the slipped surface, which may resist the slippage. However, the numerical simulation does not consider such local scratches. Although the experimental and simulation results are not in a good agreement, the model can be used for comparative purposes. Here, the model confirmed the hypothesis that there is relative movement under free loading.

In this study, to understand the phenomena essentially, the interfacial slip was verified experimentally and the elastic roll deformation effect was discussed analytically under free rolling condition. By clarifying the phenomenon in this way, such unknown failure can be prevented and the sleeve assembly type roll can be used much more widely. Although the driving torque may promote the interfacial slip, it is essential that the phenomena can be realized under free rolling in this study.

6. Conclusions

Shrink-fitted sleeve rolls have several advantages in rolling although interfacial slip sometimes appears and causes the roll damage. Since there were no detail studies are available, in this study, numerical and experimental simulations were performed to clarify the phenomenon of the irreversible relative displacement. Under free rolling condition that is similar to ball bearing, the effect of roll deformation on the circumferential slippage was discussed. The irreversible relative displacement was focused, which is corresponding to the interfacial slip in ball bearing. The conclusions can be summarized as follows:

1) In the numerical simulation, the irreversible relative displacement was confirmed by removing the external load. The accumulation of the irreversible relative displacement $u_{\theta,ave.}^{P(0)\sim P(2\pi)}$ due to the rotation force can be regarded as the slip per rotation since the order of the experiment agrees with the simulation results.
2) The interfacial displacement is promoted by the roll deformation since $u_{\theta,ave.}^{P(0)\sim P(\varphi)}$ increases with decreasing the shaft Young's modulus E_{shaft} as shown in Fig. 5. The effect of E_{shaft} on the irreversible relative displacement is related to the interface slippage region size ℓ_{slip} as shown in Fig. 7.
3) The interface slippage region ℓ_{slip} can be explained from the smaller contact stress region ℓ_{small} as shown in Fig. 9. This is because as the smaller contact stress region size ℓ_{small} becomes larger, the slippage may occur easily. The smaller stress region increases with decreasing shaft Young's modulus E_{shaft} as shown in Fig. 10.

In this study, the interfacial slip was confirmed under free rolling condition. It is crucial to understand that the interfacial slip appears due to the elastic roll deformation even under no driving torque. By clarifying the phenomenon in this way, such unknown failure can be prevented, and the sleeve assembly type roll can be used much more widely, the authors believe.

Declaration of Competing Interest

The authors declare that they have no known competing financial interests or personal relationships that could have appeared to influence the work reported in this paper.

Appendix A:. Interfacial displacement $u_{\theta}^{P(0)\sim P(\varphi)}(\theta)$ and average interfacial displacement $u_{\theta,ave.}^{P(0)\sim P(\varphi)}(\theta)$

Fig. A.1 illustrates two-dimensional modelling where the roll rotation is expressed by the load shifting on the fixed roll surface [12–15]. The roll is assumed to be subjected to the concentrated rolling load $P = 13270$ N/mm [4,5]. As shown in Fig. A.1, the continuous roll rotation can be expressed by the discrete load shifting with a constant interval φ_0. The most suitable value of φ_0 can be chosen to reduce the computational time without loosening the accuracy. From the comparison among the results $\varphi_0 = 0.25^\circ \sim 12^\circ$, the load shift angle $\varphi_0 = 4^\circ$ is adopted in the following discussion since the relative error between $\varphi_0 = 0.25^\circ$ and $\varphi_0 = 4^\circ$ is less than a few percent. In the following, both forces are denoted by P.

Fig. A.2 shows the variation of $u_{\theta}^{P(0)}(\theta)$ due to the initial load $P(0)$ by comparing the elastic and rigid shaft. As shown in Fig. A.2a, the displacement is symmetric with respect to $\theta = 0$ as can be expressed in the following equation:

$$-u_{\theta}^{P(0)}(-\theta) = u_{\theta}^{P(0)}(\theta) \tag{A.1}$$

Fig. A.2b shows the displacement $u_{\theta}^{P(0)\sim P(\pi)}(\theta)$ for the elastic shaft due to the load shifting $P(0) \sim P(\pi)$ and the displacement

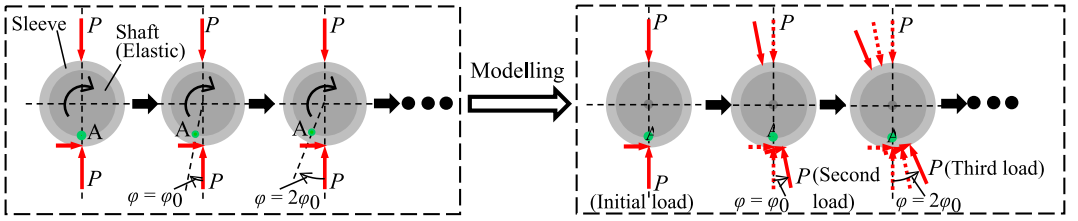

(a) Rotation of the real roll. (b) Rotation of the loads in the FEM model.

Fig. A.1. The roll rotation can be replaced by discrete load shifting by the angle φ_0 on the fixed roll.

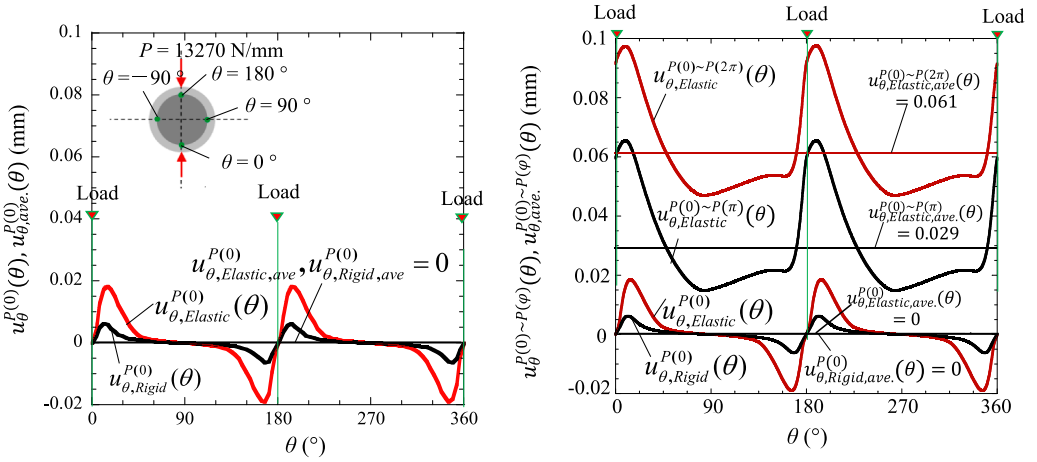

(a) Displacement $u_{\theta}^{P(0)}(\theta)$ due to the initial loading $P(0)$.

(b) Displacement $u_{\theta}^{P(0)\sim P(\varphi)}(\theta)$ due to loading shift $P(0)\sim P(\pi)$ and $P(0)\sim P(2\pi)$.

Fig. A.2. Variations of the interfacial displacement.

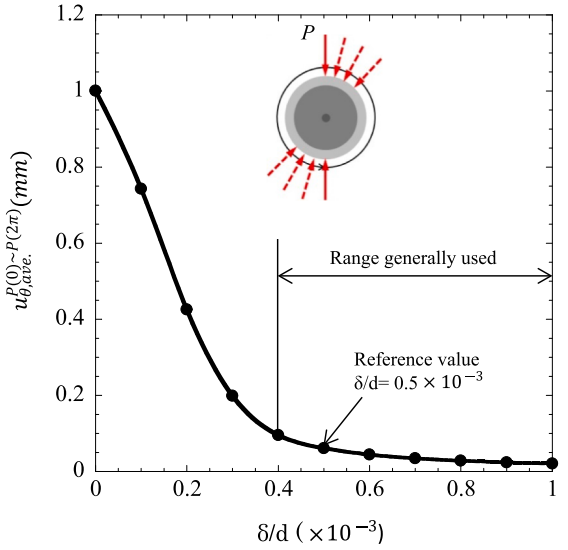

Fig. B.1. Average displacement vs. δ/d when the load shifting angle$\varphi = 0 \sim 2\pi$.

$u_\theta^{P(0)\sim P(2\pi)}(\theta)$ due to the load shifting $P(0) \sim P(2\pi)$ in comparison with $u_\theta^{P(0)}(\theta)$. As shown in Fig. A.2b, $u_\theta^{P(0)\sim P(\pi)}(\theta)$ and $u_\theta^{P(0)\sim P(2\pi)}(\theta)$ are not symmetric anymore with respect to $\theta = 0$ due to the load shifting as given in the following equation:

$$-u_\theta^{P(0)\sim P(2\pi)}(-\theta) \neq u_\theta^{P(0)\sim P(2\pi)}(\theta) \tag{A.2}$$

In Fig. A.2a and b, the average values of the displacements are also indicated by $u_{\theta,ave.}^{P(0)}$ and $u_{\theta,ave.}^{P(0)\sim P(\varphi)}$. Since those displacement varies depending on θ, the average displacement can be defined as follows:

$$u_{\theta,ave.}^{P(0)\sim P(\varphi)} = \frac{1}{2\pi}\int_0^{2\pi} u_\theta^{P(0)\sim P(\varphi)}(\theta)d\theta \tag{A.3}$$

When the initial load P is applied at $\varphi = 0$, the average displacement is zero as $u_{\theta,ave.}^{P(0)} = 0$ and $u_\theta^{P(0)}(\theta)$ is symmetric. Due to the load shifting from $\varphi = 0$ to $\varphi = \varphi$, the average displacement $u_{\theta,ave.}^{P(0)\sim P(\varphi)}$ increases losing the symmetry. This is because $u_\theta^{P(0)}(\theta)$ is irreversible as shown in Fig. 3.

Appendix B:. Effect of shrink-fitting ratio δ/d on the interfacial slip

In this paper, the shrink-fitting ratio $\delta/d = 0.5 \times 10^{-3}$ is focused to clarify the effect of the elastic deformation on the interface slippage. Usually, the shrink-fitting ratio in the range $\delta/d = 0.4 \times 10^{-3} \sim 1.0 \times 10^{-3}$ is applied to sleeve rolls on the basis of long year experience. This is because a smaller value $\delta/d < 0.4 \times 10^{-3}$ may cause interface slip easily and a larger value δ/d greater than 1.0×10^{-3} may increase the risk of sleeve fracture [6]. Fig. B.1 indicates the average displacement after one rotation $u_{\theta,ave.}^{P(0)\sim P(2\pi)}$ by varying the shrink-fitting ratio δ/d. The displacement $u_{\theta,ave.}^{P(0)\sim P(2\pi)}$ decreases with increasing δ/d. This is because with increasing δ/d, the shrink-fitted stress $\sigma_{r_{shrink}}$ increases and the slip resistance also increases on the fitting surface. Even when $\delta/d \to 0$, $u_{\theta,ave.}^{P(0)\sim P(2\pi)}$ does not go to infinity because of the contact of the sleeve and the shaft due to the load P causing the slip resistance at the contact portion. On the other hand, when $\delta/d \to \infty$, the sleeve and the shaft are integrated together and $u_{\theta,ave.}^{P(0)\sim P(2\pi)} \to 0$. Care should be taken for the large circumferential stress σ_θ at the inner surface which may cause the fracture when the larger shrink-fitting ratio is applied.

References

[1] H. Shimoda, S. Onodera, K. Hori, Study on the residual deflection of large sleeved back-up rolls: 4th Report, Residual stresses of sleeved rolls, Trans. Jpn. Soc. Mech. Eng. 32 (1966) 689–694.
[2] T. Irie, K. Takaki, I. Tsutsunaga, Y. Sano, Steel strip and section steel and thick rolling, processing, Tetsu-to-Hagane 65 (1979) 293.
[3] H. Takigawa, K. Hashimoto, G. Konno, S. Uchida, Development of forged high-speed-steel roll for shaped steel, CAMP-ISIJ 16 (2003) 1150–1153.
[4] Y. Sano, Recent advances in rolling rolls. Proc of the No. 148–149 Nishiyama Memorial Technology Course, Tokyo, Japan (1993) 193–226.
[5] Y. Sano, Fatigue failure problem in the inside of roll body for hot strip rolling- Crack initiation problem and its estimation in the actual plant, in: The 245th JSMS Committee on Fatigue of Materials and The 36th JSMS Committee on Strength Design, Safety Evaluation, 1999, p. 40.
[6] E. Matsunaga, T. Tsuyuki, Y. Sano, Optimum shrink fitting ratio of sleeve roll (Strength design of shrink fitted sleeve roll for hot strip mill-1), CAMP-ISIJ 11 (1998) 362. https://ci.nii.ac.jp/naid/10002551803.
[7] S. Tutumi, S. Hara, S. Yoshi, The residual deflection of sleeved backup-up rolls, Tetsu-to-Hagane 57 (5) (1971) 818–822.
[8] S. Spuzic, K.N. Strafford, C. Subramanian, G. Savage, Wear of hot rolling mill rolls: an overview, Wear 176 (2) (1994) 261–271, https://doi.org/10.1016/0043-1648(94)90155-4.
[9] N.-A. Noda, K. Hu, Y. Sano, K. Ono, Y. Hosokawa, Residual stress simulation for hot strip bimetallic roll during quenching, Steel Res. Int. 87 (11) (2016) 1478–1488, https://doi.org/10.1002/srin.v87.1110.1002/srin.201500430.
[10] N.A. Noda, Y. Sano, Y. Takase, Y. Shimoda, G. Zhang, Residual deflection mechanism for back-up roll consisting of shrink-fitted sleeve and arbor, J. JSTP 58 (2017) 66.
[11] K. Hu, Y. Xia, F. Zhu, N.-A. Noda, Evaluation of thermal breakage in bimetallic work roll considering heat treated residual stress combined with thermal stress during hot rolling, Steel Res. Int. 89 (4) (2018) 1700368, https://doi.org/10.1002/srin.v89.410.1002/srin.201700368.
[12] N.A. Noda, H. Sakai, Y. Sano, Y. Takase, Y. Shimoda, Quasi-equilibrium stress zone with residual displacement causing permanent slippage in shrink-fitted sleeve rolls, Metals 8 (12) (2018) 998, https://doi.org/10.3390/met8120998.
[13] H. Sakai, N.A. Noda, Y. Sano, G. Zhang, Y. Takase, Effect of driving torque on the interfacial creep for shrink-fitted bimetallic work roll, Tetsu-to-Hagane 105 (12) (2019) 1126–1134, https://doi.org/10.2355/tetsutohagane.TETSU-2019-048.
[14] H. Sakai, N.A. Noda, Y. Sano, G. Zhang, Y. Takase, Numerical simulation on interfacial creep generation for shrink-fitted bimetallic work roll, Tetsu-to-Hagane 105 (2019) 411–417, https://doi.org/10.2355/tetsutohagane.TETSU-2018-117.
[15] H. Sakai, N.A. Noda, Y. Sano, G. Zhang, Y. Takase, Numerical simulation on interfacial creep generation for shrink-fitted bimetallic roll, ISIJ Int. 59 (5) (2019) 889–894, https://doi.org/10.2355/isijinternational.ISIJINT-2018-749.
[16] N. Soda, Bearing, Tokyo, Iwanami Shoten, 1964, pp. 196–203.
[17] Imai: Lubrication, 4 (1959) 307.
[18] J. Murata, T. Onizuka, Generation mechanism of inner ring creep, Koyo Eng. J. 166 (2005) 41–47.
[19] T. Niwa, A creep mechanism of rolling bearings, NTN Tech. Rev. 81 (2013) 100–103.
[20] Sakajiri Ten, Yukawa Takemura, NSK Tech. J. 680 (2006) 13.
[21] New Bearing Doctor: Diagnosis of bearing problems. Objective: Smooth & reliable operation. NSK (1997). https://www.nsk.com/common/data/ctrgPdf/e7005c.pdf.
[22] J. Zhan, H. Takemura, K. Yukawa, A study on bearing creep mechanism with FEM simulation, Proc. of IMECE2007 (2007), https://doi.org/10.1115/IMECE2007-41366. Seattle, Washington, USA.
[23] Jianjun Zhan, Kinji Yukawa, Hiromichi Takemura, in: Advanced Tribology, Springer Berlin Heidelberg, Berlin, Heidelberg, 2010, pp. 237–238, https://doi.org/10.1007/978-3-642-03653-8_74.

[24] S. Noguchi, K. Ichikawa, A study about creep between inner ring of ball bearing and shaft, in: Proceeding of Academic Lectures of the Japan Society for Precision Engineering, 2010, Japan. https://doi.org/10.11522/pscjspe.2010A.0.565.0.
[25] T. Teramoto, Y. Sato, Prediction method of outer ring creep phenomenon of ball bearing under bearing load, Trans. Of Society of Automotive Eng. of Japan 46 (2015) 355–360, https://doi.org/10.11351/jsaeronbun.46.355.
[26] C. Bovet, L. Zamponi, An approach for predicting the internal behaviour of ball bearings under high moment load, Mech. Mach. Theory 101 (2016) 1–22, https://doi.org/10.1016/j.mechmachtheory.2016.03.002.
[27] A. Maiwald, E. Leidich, FE simulations of irreversible relative movements (creeping) in rolling bearing seats –Influential parameters and remedies, in: World Congress on Engineering and Computer Science 2013 Vol II, San Francisco, USA. http://www.iaeng.org/publication/WCECS2013/WCECS2013_pp1030-1035.pdf.
[28] T. Schiemann, S. Pörsch, E. Leidich, B. Sauer, Intermediate layer as measure against rolling bearing creep, Wind Energy 21 (6) (2018) 426–440, https://doi.org/10.1002/we.v21.610.1002/we.2170.
[29] T. Miyazaki, N.A. Noda, F. Ren, Z. Wang, Y. Sano, K. Iida, Analysis of intensity of singular stress field for bonded cylinder and bonded pipe in comparison with bonded plate, Int. J. Adhes. Adhes. 77 (2017) 118–137, https://doi.org/10.1016/j.ijadhadh.2017.03.019.
[30] N.A. Noda, T. Miyazaki, R. Li, T. Uchikoba, Y. Sano, Y. Takase, Debonding strength evaluation in terms of the intensity of singular stress at the interface corner with and without fictitious crack, Int. J. Adhes. Adhes. 61 (2015) 46–64, https://doi.org/10.1016/j.ijadhadh.2015.04.005.
[31] N.A. Noda, T. Uchikoba, M. Ueno, Y. Sano, K. Iida, Z. Wang, G. Wang, Convenient debonding strength evaluation for spray coating based on intensity of singular stress, ISIJ Int. 55 (12) (2015) 2624–2630, https://doi.org/10.2355/isijinternational.ISIJINT-2015-458.
[32] Zefeng Wang, Nao-Aki Noda, Masayasu Ueno, Yoshikazu Sano, Optimum design of ceramic spray coating evaluated in terms of intensity of singular stress field, Steel Res. Int. 88 (7) (2017) 1600353, https://doi.org/10.1002/srin.v88.710.1002/srin.201600353.
[33] N.A. Noda, X. Chen, Y. Sano, M.A. Wahab, H. Maruyama, R. Fujisawa, Y. Takase, Effect of pitch difference between the bolt-nut connections upon the anti-loosening performance and fatigue life, Mater. Des. 96 (2016) 476–489, https://doi.org/10.1016/j.matdes.2016.01.128.
[34] N.A. Noda, R. Takaki, Y. Shen, A. Inoue, Y. Sano, D. Akagi, Y. Takase, P. Galvez, Strain rate concentration factor for flat notched specimen to predict impact strength for polymeric materials, Mech. Mater. 131 (2019) 141–157, https://doi.org/10.1016/j.mechmat.2019.01.011.
[35] Shintarou MATSUDA, Dedi SURYADI, Nao-Aki NODA, Yoshikazu SANO, Yasushi TAKASE, Shota HARADA, Structural design for ceramics rollers used in the heating furnace加熱炉中セラミックローラーの構造設計に関する研究, Trans. JSME Ser. A 79 (803) (2013) 989–999.
[36] N.A. Noda, D. Suryadi, S. Kumasaki, Y. Sano, Y. Takase, Failure analysis for coming out of shaft from shrink-fitted ceramics sleeve, Eng. Fail. Anal. 57 (2015) 219–235, https://doi.org/10.1016/j.engfailanal.2015.07.016.
[37] N.A. Noda, Y. Xu, D. Suryadi, Y. Sano, Y. Takase, Coming out mechanism of steel shaft from ceramic sleeve, ISIJ Int. 56 (2) (2016) 303–310, https://doi.org/10.2355/isijinternational.ISIJINT-2015-558.
[38] G. Zhang, H. Sakai, N.A. Noda, Y. Sano, S. Oshiro, Generation mechanism of driving out force of the shaft from the shrink fitted ceramic roll by introducing newly designed stopper, ISIJ Int. 59 (2) (2019) 293–299, https://doi.org/10.2355/isijinternational.ISIJINT-2018-615.
[39] Marc Mentat team, Theory and User Information Vol. A (2008) 713.
[40] Misumi-vona Top, Technical information, Dry coefficient of friction. https://jp.misumi-ec.com/tech-info/categories/plastic_mold_design/pl07/c0874.html.